Hindawi
Shock and Vibration
Volume 2019, Article ID 9641478, 15 pages
https://doi.org/10.1155/2019/9641478

Research Article

Detection of Inception Cavitation in Centrifugal Pump by Fluid-Borne Noise Diagnostic

Liang Dong[1,2] **Yuqi Zhao**,[1] **and Cui Dai**[3]

[1]*Research Center of Fluid Machinery Engineering and Technology, Jiangsu University, Zhenjiang 212013, China*
[2]*Sichuan Provincial Key Lab of Process Equipment and Control, Sichuan University of Science & Engineering, Zigong 643000, China*
[3]*School of Energy and Power Engineering, Jiangsu University, Zhenjiang 212013, China*

Correspondence should be addressed to Cui Dai; daicui@ujs.edu.cn

Received 21 November 2018; Accepted 14 February 2019; Published 26 March 2019

Academic Editor: Radoslaw Zimroz

This paper presents an experimental methodology that is capable of sensitively detecting the cavitation inception in a centrifugal pump. Firstly, with a centrifugal pump of n_s = 117 as research object, the cavitation performance, the bubble pattern distribution at impeller inlet, and the vibration and noise were synchronously measured at different flow conditions each with several cavitation coefficients. The change laws of total level of vibration and noise signals throughout the cavitation process were emphatically investigated. After comparing the sensitivity and reliability of different detection methods, the method based on overall sound pressure level of liquid-borne noise is found to present high sensitivity to cavitation. Secondly, by comparing the affected 1/3 octave spectrum by changing flow and cavitation coefficients, the highly sensitive frequency band to cavitation was obtained. Then, a new inception cavitation detection method was proposed based on Pauta principle. Finally, the method was verified through an ultra-low-specific speed pump (n_s = 25). The results show that the total pressure level of liquid-borne noise increases firstly and then decreases with the development of cavitation. The broadband SPL of liquid-borne noise between 2000 and 3000 Hz can be used to detect the inception cavitation, and the cavitation detection threshold is determined as 1.0%.

1. Introduction

Centrifugal pumps are widely used in various engineering applications, such as agriculture, industry, drainage, and others [1]. With the development for high speed, the pump cavitation has become one major issue that causes negative effect on the operation stability [2]. Although the occurrence of cavitation can be effectively restrained by reasonable design or inlet supercharging, it cannot be eliminated fundamentally [3, 4].

At present, there are several methods for detecting cavitation inception that are the energy method [5], optical method [6], surface coating method [7], electrical resistance method [8], acoustic emission technology [9, 10], and vibroacoustic method [11, 12]. With a head drop of 3% or an efficiency drop of 1% as the criterion, the energy method could cause an erroneous estimate because actually the cavitation has developed to a certain extent under these conditions. The optical method is suitable for capturing the development state of cavitation when conducting a model test. Owing to high experimental cost and on-site condition limit for actual pump, its usage range is greatly narrowed. Covered with a layer material vulnerable to cavitation erosion on the surface of flow components, the surface coating method can directly observe the damage position and degree. However, it could not be well applied for most industrial applications due to the need for shutdown detection. The electrical resistance method mainly consists of direct and indirect methods. The former can determine the cavitation damage degree through comparing the resistance values of the metal sheet attached on the surface of flow component before and after cavitation, while the latter can only determine the relative strength of cavitation by measuring the resistance change of liquid medium. Owing to low signal robustness, the accuracy of the two methods cannot be guaranteed.

These years, many researches begin to focus on the acoustic emission technology and the vibroacoustic method.

Acoustic emission technology has high requirements on background noise, so the environmental factor has become an important reason to restrict its wide application. The vibroacoustic method has received extensive attention from domestic and foreign scholars because of its real-time performance, strong anti-interference, lower operation cost, and wider acceptance. Bajic and Keller [13, 14] conducted a series of experiments for early detection of cavitation in a hydro turbine by the vibroacoustic diagnostics. With a certain number of accelerometers and sound pressure gauges installed on the guide vane, cover, and draft tube, the cavitation location on the impeller blade was obtained. It was found that the peak waveform between 80 and 100 kHz can reflect the shock response characteristic of high-frequency band existed in the cavitation signal. Through the normalized spectrum calculated from the power spectral density function, the cavitation signal can be compensated while the resonance signal can be suppressed. Friedrich [15] experimentally investigated the variation of cavitation noise in the whole process of cavitation on a visual test bench. During the experiment, the cavitation noise signal with higher signal-to-noise ratio was obtained after weakening the background noise by using signal cancellation technology. In the research of Čudina and Prezelj [16, 17], a specific frequency of 147 Hz in the noise spectrum was found to be related to the cavitation inception of a pump. And it is more accurate than the traditional predicting method of 3% head drop. However, this conclusion has not been confirmed in the research studies of other scholars. Rus et al. [18] measured the vibration and noise signals caused by cavitation in a two-blade axial-flow turbine and proved that there is a certain correlation between them. Escaler et al. [19] conducted the resonance and dynamic pressure tests on a scaled model of mixed flow turbine under various cavitation conditions. Through frequency domain analysis, it was found the cavitation signals are concentrated in the frequency band of 10–100 kHz, and the frequencies from 10 Hz to 15 kHz are more suitable for high-frequency component analysis. In addition, it is proposed that different kinds of sensors and detecting methods are needed for various cavitation types. The attached cavitation spectrum is concentrated around 10 kHz and the measuring points should be placed close to the impeller. The bubble cavitation spectrum is concentrated at 3 kHz and is related to radial vibration of the bearing. The vortex cavitation spectrum is concentrated between 30 and 40 kHz, and it is appropriate for determination though using dynamic pressure sensor. Duan et al. [20] collected and processed the vibration and noise signals of a water-jet propulsion pump. Based on the peak sequence of the second derivative of the cavitation feature band, the feature sets were constructed to jointly identify the cavitation. Finally, the cavitation stage was divided into three stages that are noncavitation stage, 1st cavitation stage, and 2nd cavitation stage. Su et al. [21] identified the cavitation status based on the vibration signals on the casing and higher derivatization of the noise signals in the inlet of a water-jet propulsion pump. Pu et al. [22] proposed a theory based on wavelet singularity to avoid the mutability of cavitation signals during morphological transformation. Shi et al. [23] summarized the characteristics of the wavelet basis functions, which are suitable for cavitation determination. To solve the blindness problem in the wavelet packet decomposition, a method of interval wavelet packet decomposition was proposed.

Note that in those studies, most of them are focused on extracting the cavitation-related vibration and noise signals by some means. And there is not a universal method for the detection of cavitation inception in centrifugal pumps. So in the paper, the frequency spectrum of vibration and noise is captured, aiming at proposing a highly sensitive cavitation detection method for a centrifugal pump.

2. Experimental System

2.1. Test Rig. A test rig was constructed in the Research Centre of Fluid Machinery Engineering and Technology, Jiangsu University, as illustrated in Figure 1. The experimental system mainly consists of a centrifugal pump connected with a transparent water tank, a vacuum pump, a cavitation tank, a pressure stabilizer, an exhaust port, inlet and outlet pipes, inlet and outlet valves, a variable-frequency driving motor, and others. Installed at the pump outlet, there is a pressure stabilizer for stabilizing the fluid pressure in the system and preventing the temperature rise due to the thermodynamic effect caused by cavitation. Besides, during the testing of liquid-borne noise, the pressure stabilizer can play the role of sound insulation and noise elimination with improved acoustic impedance. Also, it can solve the resonance and frequency-interference problems between the noise generated by the change of flowmeter and valve opening in the downstream of pressure stabilizer and the cavitation-induced noise of the pump. To reduce the interference from the system vibration, the tested pump and motor are fixed on the huge base, and the thick rubber gaskets are used at the connections between the pipeline and the pump. The thickness of the inlet and outlet pipes is chosen to be 8 mm for suppressing the Poisson coupling.

Before the testing, the valves in the closed loop system (valves 1, 2, and 3) were open. The cavitation tank was filled with water through the injection hole, and it was closed once there was water flowing out from the exhaust port of pressure stabilizer. Then, the air valve of cavitation tank was open to connect with the atmosphere. In the meantime, the centrifugal pump started to operate for a period to discharge the air in the system and eventually to make the pressure of the loop system remain stable. The pump can stably operate at certain rotating speed and flow condition, respectively, by adjusting the variable-frequency driving motor and the opening degree of valve 3. The fluid through the valve 3 has pressure loss, which leads to pressure difference between the cavitation tank and pressure stabilizer. After that, by lowering the pressure in the cavitation tank controlled by the vacuum pump, the inlet pressure of centrifugal pump was reduced to present different cavitation stages. Furthermore, at some rotating speed and flow conditions, the air bubble distribution at the impeller inlet and the vibration and noise signals can be collected synchronously under different cavitation coefficients.

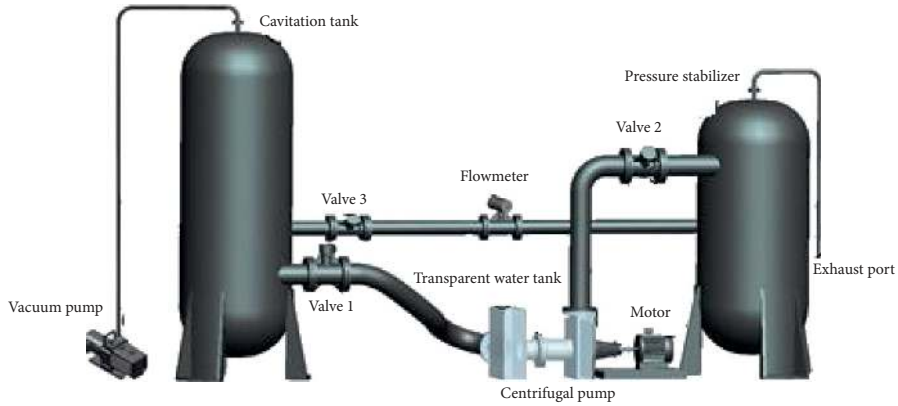

Figure 1: Schematic of test rig.

2.2. High-Speed Photography. The tested model is a medium-specific speed volute-type centrifugal pump. The performance parameters at the design point are $Q_d = 40\,m^3/h$, $H = 8\,m$, $n = 1450$ r/min, and $n_s = 117$. The main geometry parameters of model pump are shown in Table 1. For the cavitation observation, both the impeller and volute casing were manufactured of organic glass. To make the cavitation bubble display clearer when shooting, the impeller was painted black with spray. Because the pump cover was made of thick metal plate, considering the pressure inside pump body and the strength of organic glass, it was sealed with rubber ring and fixed with C clamp. With a standard mechanical seal installed on the shaft, owing to the influence of the airtightness of mechanical seal on the pressure retention of test system, "O" seal ring was adopted between the moving ring and shaft and between the static ring and casing. The physical drawings of pump body, pump cover, and impeller are shown in Figure 2.

The cavitation inside centrifugal pump firstly occurs on the suction surface of impeller inlet. For capturing the complete bubble pattern at impeller inlet, a sealed transparent water tank is put up. The water tank is placed on the side of pump inlet, and the high-speed camera is directly positive to the tank. In addition, a row of air holes is arranged on the top, which is convenient to discharge the gas from the system when adding and discharging water and to maintain the pressure stability. For stabilizing the flow in pump inlet, its volume was designed to be $0.1\,m^3$. The cavitation at the impeller inlet was collected by MotionPro Y4 high-speed CMOS digital camera produced by IDT Company in the United States. Two LED lights were adopted to increase the brightness of the impeller inlet during shooting. The LED light is a cold light source, which will not affect the fluid temperature. When shooting, the light source was placed on both sides of the inlet pipe to avoid the local shadow caused by a single light source. The shooting speed was set to 3000 frames per second.

2.3. Vibration and Noise Measurements. A INV3020C high-performance data acquisition system, combined with acceleration and sound pressure transducers, was used to measure the signals of solid-borne vibration, liquid-borne noise, and airborne noise. The acceleration transducer incorporated one type of INV9822A with a sampling frequency range of 0.5–8 kHz. For the vibration measurements, 5 monitoring points (M_1–M_5) were located, respectively, on the pump foot, discharge flange, and pump casing. The sound pressure sensor of INV 9206 was placed 1m away from the impeller inlet, with a resolution of ±0.2 dB. For the liquid-borne noise measurement, a RHSA-10 hydrophone was used, whose sampling frequency range was from 20 Hz to 100 kHz with a resolution of ±2 dB. The flush method can reliably measure the pulsating sound field in the pipe [24]. The flush method is employed for hydrophone setups. Owing to easy influence from the pressure fluctuation of pump outlet, the hydrophone was flush mounted at 8 times of outlet diameter from the discharge flange. Different from the spectrum distribution of mechanical failure signal, the broadband feature under cavitation reflects both in low- and high-frequency bands. To ensure the spectral precision in low-frequency band and reflect the changing trend in high-frequency band, the vibration and noise signals were collected for 30 s with a sampling frequency of 12.8 kHz.

Table 1: Main geometry parameters of model pump.

Items	Parameters	Values
Impeller	Inlet diameter, D_1 (mm)	90
	Outlet diameter, D_2 (mm)	170
	Number of blades, z	6
	Wrap angle, θ (°)	120
	Outlet width, b_2 (mm)	13
Volute	Basic diameter, D_3 (mm)	180
	Inlet width, b_3 (mm)	32
	Discharge diameter, D_4 (mm)	80

The instruments used in the measuring system for the vibration and noise are given in Table 2. The installation locations of the sensors are shown in Figure 3.

3. Experimental Results at Rated Rotating Speed

3.1. Cavitation Performance. To investigate the cavitation performance of the pump at rated rotating speed of 1450 r/min, the flow coefficient φ, head coefficient ψ, and cavitation coefficient σ are analyzed. They are defined as follows:

(a) (b) (c)

Figure 2: Physical drawings of (a) pump body, (b) pump cover, and (c) impeller.

Table 2: Instruments in measuring system.

Device	Range	Resolution	Locations
Electromagnetic flowmeter	1–50 m^3/h	±0.5%	The length of straight pipe before and after the flowmeter is 10 times of its internal diameter
Pressure transducer at inlet	−0.1–0.1 MPa	±0.5%	2 times of pipe diameter from inlet flange
Pressure transducer at outlet	0–0.1 MPa	±0.5%	2 times of pipe diameter from outlet flange
Vibration acceleration transducer	0.5–8 kHz	10 Mv/ms^{-2}	Discharge flange, pump foot, and pump casing
Sound pressure transducer	20 Hz–100 kHz	±0.2 dB	1 m away from impeller inlet
Hydrophone	20 Hz–200 kHz	±2 dB	8 times of pipe diameter from outlet flange

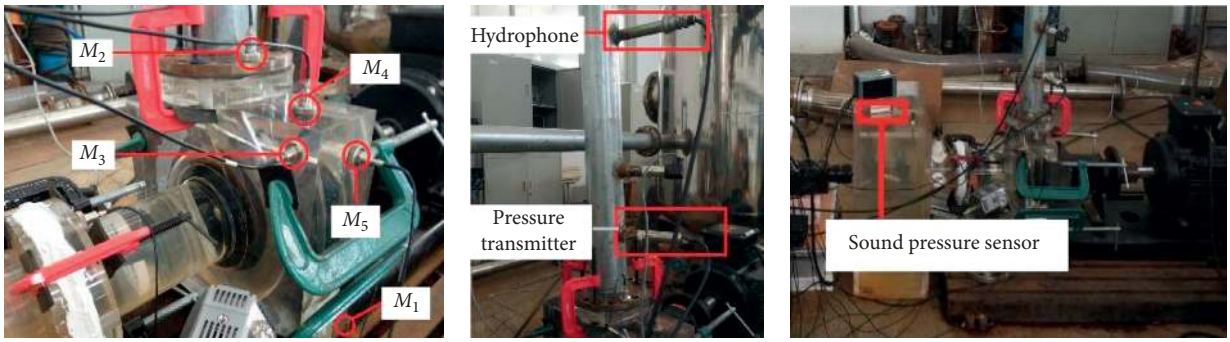

(a) (b) (c)

Figure 3: Locations of monitoring points for vibration and noise measurement: (a) solid-borne vibration; (b) liquid-borne noise; (c) airborne noise.

$$\varphi = \frac{Q}{\pi D_2 b_2 n},$$
$$\psi = \frac{H}{u_2^2/2g}, \quad (1)$$
$$\sigma = \frac{P_{in} - P_v}{0.5\rho_l u_2^2},$$

where D_2 is the outlet diameter of impeller, b_2 is the outlet width of impeller, n is the rotating speed, u_2 is the circumferential velocity at the impeller outlet, g is the gravitational acceleration, P_{in} is the pressure at impeller inlet, p_v is the saturated vapor pressure ($p_v = 3574$ Pa), and ρ_l is the medium density ($\rho_l = 998\ kg/m^3$).

The cavitation performance curves of the tested pump for three flow coefficients are shown in Figure 4 as a function of cavitation coefficient. And it is generally believed the cavitation is fully developed when the head drops about 3% on the basis of the traditional energy method. The corresponding critical cavitation number is defined as σ_c. At the flow coefficient of 0.065, the critical cavitation coefficient is observed to be located at 0.297. The critical cavitation coefficients for three flow coefficients are shown in Table 3, which exhibits an obvious influence caused from the flow, namely, the higher the flow coefficient, the higher the critical cavitation coefficient.

3.2. High-Speed Photography. The cavitation bubble distribution at the impeller inlet for three flow coefficients is

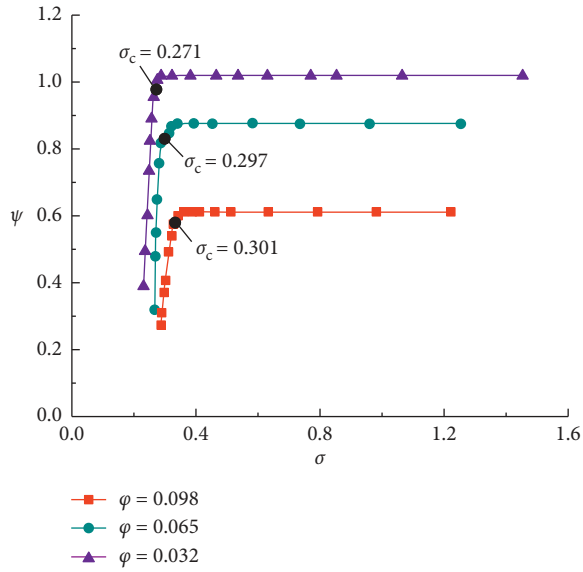

Figure 4: Cavitation performance curves at rated rotating speed.

Table 3: Critical cavitation coefficient based on the energy method.

Flow coefficient φ	0.032	0.065	0.098
Critical cavitation coefficient σ_c	0.271	0.297	0.301

displayed in Figures 5–7. In Figure 6, at the cavitation coefficients of 1.384 and 0.338, the pump runs normally without cavitation bubble captured at the impeller inlet. When it reduces to 0.321, a small amount of bubbles are firstly found at the suction surface of blade. At the moment, the corresponding cavitation coefficient obtained through the high-speed photography is seen as the visible incipient cavitation coefficient, denoted by σ_p. Compared with Figure 4, the visible incipient cavitation coefficient σ_p is larger than the critical cavitation coefficient σ_c, which indicates the pump head has not changed yet when the cavitation begins to occur. Note that at the time, the cavitation bubble does not appear on each blade simultaneously, mainly due to the pressure distribution unevenly distributed in flow passages caused by the asymmetric structure of volute and tongue. When the cavitation coefficient reduces to the critical cavitation coefficient σ_c of 0.297, the cavitation already arises nearly on each blade and the connected bubble area appears when it is less than σ_c.

Also, seen from Figure 4, the head coefficients remain constant at 1.03 and 0.62, respectively, for $\varphi = 0.032$ and $\varphi = 0.098$ at the condition of visible incipient cavitation, which further proves that the hydraulic performance of the pump is not affected when the cavitation initially occurs. In Figures 5 and 7, under smaller and larger flow conditions, the cavitation is already evident at their critical cavitation coefficients. As the cavitation coefficient continues to decline, a small number of traveling cavitation bubbles not attached on blade surface begin to appear. At the time, the bubble area at the suction surface of pump inlet remains basically unchanged, while the bubble thickness cannot be confirmed only from the shooting direction. Therefore, it is unable to further distinguish the difference of cavitation degree only by high-speed photography. On the other hand, although the cavitation detection based on the optical method is more accurate, due to low practicability in practical engineering applications, other cavitation detection methods are needed. The visible incipient cavitation coefficients for three flow coefficients are shown in Table 4, further suggesting the cavitation is more easily to happen for higher flow rate.

3.3. Liquid-Borne Noise, Airborne Noise, and Solid-Borne Vibration. The traveling cavitation bubble cluster would affect the internal flow inside the pump, which can be reflected in the form of sound energy. On the other hand, the pressure wave formed by the collapse of cavitation bubbles would firstly act on the liquid, which in turn generate liquid-borne noise. The background noise was measured and the overall sound pressure level (OSPL) is much smaller than that of the pump, which can be negligible in the paper. The OSPL curves of liquid-borne noise for three flow coefficients are demonstrated in Figure 8 in terms of cavitation coefficient. The overall sound pressure level L_p is calculated as follows:

$$L_p = 10 \log \int_{f_0}^{f_{max}} \frac{(p_a/\sqrt{2})^2}{p_0^2} df = 10 \log \sum_{i=f_0}^{f_{max}} \frac{(p_i/\sqrt{2})^2}{p_0^2} \Delta f_i, \quad (2)$$

where Δf_i is the minimum frequency resolution, f_0 and f_{max} are the frequency limits, p_a or p_i is the effective sound pressure, and p_0 is the reference sound pressure ($p_0 = 1 \times 10^{-6}$ Pa for water).

We can see that the OSPL of liquid-borne noise at $\varphi = 0.065$ is minimum at the respective cavitation coefficient under noncavitation condition. This is mainly because the higher efficiency is corresponding to relatively smaller sound pressure level for fixed total energy. As the efficiency reduces under partial working conditions, the lost energy is reflected in the form of acoustic energy, which induces higher OSPL than rated working condition. And at noncavitation stage, the OSPL of liquid-borne noise under different cavitation coefficients remains stable. For the reduction of cavitation coefficient, it can be regarded as an increase of installation height of the pump, which has no influence on internal flow. However, after certain cavitation coefficient, the OSPL of liquid-borne noise gradually increases to an extreme value and then decreases with decreasing cavitation coefficient. There are several reasons for the existence of extreme point in the OSPL curves. Firstly, under the action of low-frequency pulse and high-frequency shock wave formed due to bubble migration and collapse, the OSPL curve rises. When the cavitation develops to a certain extent, the impeller inlet or even the flow passage will be blocked by a large number of bubbles, resulting in the rapid decay of high-frequency energy and the isolation of low-frequency energy by cavitation bubble. Then, the sound pressure level measured by the sensor will decline. Besides, two-phase flow is formed due to a large amount of bubbles flowing with the medium. The compressibility of two-phase flow and the resistance of wall would rise sharply. As a result, the acoustic property of the medium

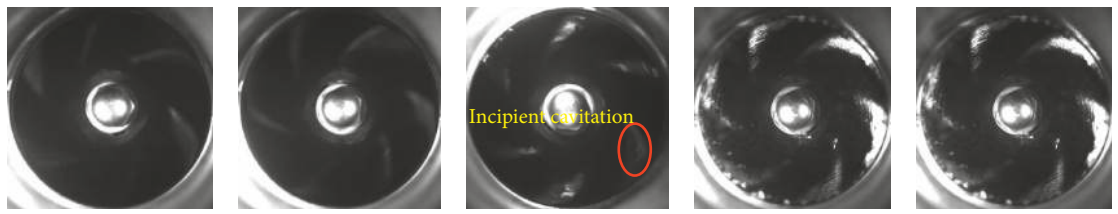

Figure 5: Cavitation pattern distribution at $\varphi = 0.032$. (a) $\sigma = 1.452$; (b) $\sigma = 0.319$; (c) $\sigma_p = 0.284$; (d) $\sigma_c = 0.271$; (e) $\sigma = 0.248$.

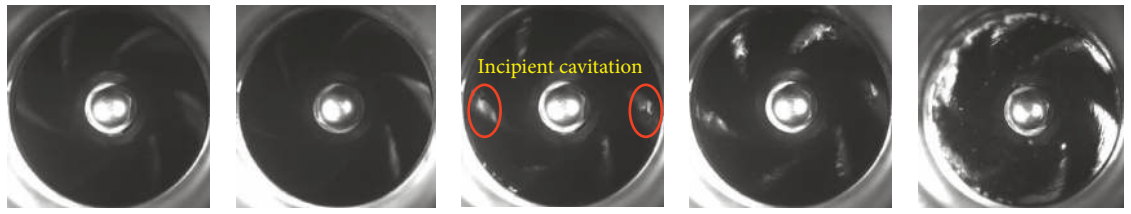

Figure 6: Cavitation pattern distribution at $\varphi = 0.065$. (a) $\sigma = 1.384$; (b) $\sigma = 0.338$; (c) $\sigma_p = 0.321$; (d) $\sigma_c = 0.297$; (e) $\sigma = 0.262$.

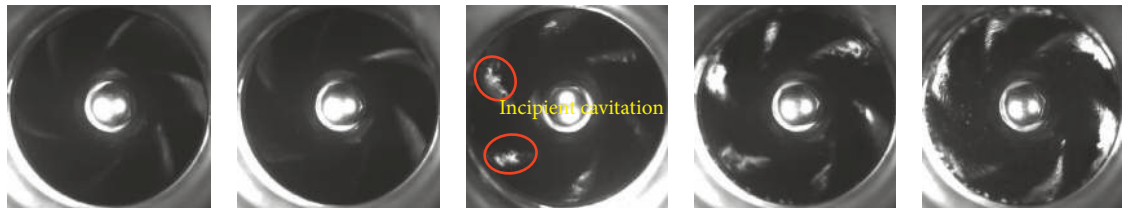

Figure 7: Cavitation pattern distribution at $\varphi = 0.098$. (a) $\sigma = 1.253$; (b) $\sigma = 0.411$; (c) $\sigma_p = 0.381$; (d) $\sigma_c = 0.301$; (e) $\sigma = 0.288$.

Table 4: Visible incipient cavitation coefficient based on high-speed photography.

Flow coefficient φ	0.032	0.065	0.098
Visible incipient cavitation coefficient σ_p	0.284	0.321	0.381

and the energy received by the sensor change. When the cavitation coefficient decreases, the expansion of bubbles would absorb the impact force and the noise caused by bubble collapse. The noise is influenced jointly by the number and collapse rate of cavitation bubbles. If the pressure decreases under constant flow rate, the noise would increase with increasing cavitation bubble number, while the noise reduces with lowering the collapse rate of cavitation bubbles.

When the cavitation inside the pump occurs, the obvious cracking sound can be felt at the test site. This is because the energy propagates in the air and radiates outward through the pipeline, pump body, and so on. The magnitude of radiation energy is positively correlated with the product of the effective root mean square value of vibrating structure and the vibration surface area. With further development of cavitation, the cracking sound will decrease. Because human ear is more sensitive to the frequency band of 800–5000 Hz, the A-weight has been conducted to airborne noise. The

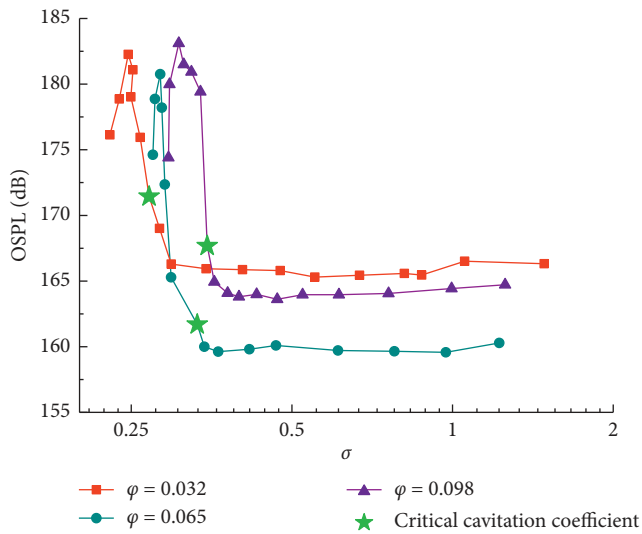

Figure 8: OSPL curve of liquid-borne noise for three flow coefficients.

OASPL curves of airborne noise for three flow coefficients are shown in Figure 9. Note that for the airborne noise, the reference sound pressure p_0 equals to 2×10^{-5} Pa.

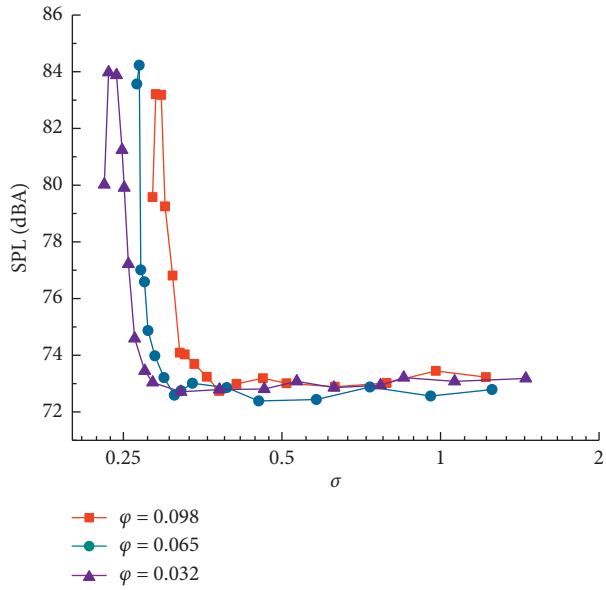

FIGURE 9: OASPL curve of airborne noise for three flow coefficients.

It is seen that for airborne noise, under noncavitation stage, there is no consistent rule but an evident fluctuation for various flow coefficients. This is maybe because the airborne noise includes not only the pump noise, but also the background noise generated by the motor, bearing, coupling, and valves. With the decrease of cavitation coefficient, the OASPL of airborne noise at higher flow coefficient of 0.098 increases, followed by the rated condition, and the lower flow condition is the latest. When the cavitation coefficient drops to a certain level, the airborne noise rises sharply until it reaches the highest point and then begins to fall.

The pressure fluctuation, cavitation-induced noise, axial and radial hydraulic forces, mechanical dynamic imbalance, and other factors would excite the solid-borne vibration in the entire system. In the test, the vibration signals of pump foot (M_1), outlet flange (M_2), pump body in axial direction (M_3), and upper and right side of pump body in radial direction (M_4 and M_5) were collected and analyzed. The vibration acceleration level (VAL) curves of solid-borne vibration for three flow coefficients are shown in Figure 10 as a function of cavitation coefficient. For nondimensionalization, the vibration acceleration level L_a is defined as follows:

$$L_a = 10 \log \frac{a_e^2}{a_0^2}, \tag{3}$$

where a_e is the effective value and a_0 is the reference value ($a_0 = 10^{-6}\,\mathrm{m/s^2}$).

Under noncavitation stage, the VAL at each measuring point fluctuates slightly but basically maintains at a lower level. The VAL at M1 is highest, where the vibration at pump foot is most intense. Comparing the three monitoring points at pump body, the VAL of M3 is observed to be larger than that of M4 and M5, indicating the flow shock is mainly concentrated in axial direction. In addition, under the cavitation coefficient larger than σ_p, the VALs of monitoring points at rated condition are smaller than those of other working conditions. Furthermore, the VALs at smaller flow coefficient of $\varphi = 0.032$ are larger than those of large flow coefficient of $\varphi = 0.098$, proving more energy is dissipated in the form of vibration at small flow condition. With the decrease of cavitation coefficient, the VALs appear to maintain a small range of fluctuations firstly and then rise sharply. After increasing to a limit, there is a small fluctuation and then the VALs appear to fall. From Figures 9 and 10, we can see that with decreasing cavitation coefficient, a maximum value for OASPL or VAL appears. This is because when the cavitation develops to a certain extent, although there is a pressure wave acting on solid wall caused by cavitation collapse, a large number of bubbles would occupy most flow passages of the pump. This will hinder the direct impact from the liquid onto solid surface, reduce the excitation force generated between the liquid and solid wall, and eventually lower the vibration level and noise level.

Owing to the sampling time of 30s, the signal can be regarded as quasisteady during the sampling period. The sound pressure level presents a certain fluctuation, but its fluctuation amount is basically less than 0.3%. With the average value of OSPL at one cavitation coefficient under noncavitation stage as the reference, the incipient cavitation coefficients based on liquid-borne noise are defined as 0.5% increase of OSPL, denoted by σ_{io}. Similarly, with the average value of OASPL as reference, the incipient cavitation coefficient based on airborne noise is defined as 0.7% increase, denoted by σ_{eo}. With the average value of VAL under noncavitation stage as the reference, the incipient cavitation coefficient based on solid-borne vibration is defined as 0.5% increase of vibration level, denoted by σ_{so}. The incipient cavitation coefficients corresponding to liquid-borne noise, airborne noise, and solid-borne vibration for three flow coefficients are shown in Table 5.

3.4. Sensitivity and Reliability Comparison. The sensitivity and reliability of cavitation detection methods are compared in Figure 11. The corresponding incipient cavitation coefficient is used to reflect the sensitivity, tagged by black mark. The higher the black mark is, the higher sensitive the detection method shows. The maximum relative deviation on the basis of reference value is calculated separately to reflect the reliability of detection methods, represented by red bars.

It can be seen that the incipient cavitation coefficient obtained by different detection methods is different, and the rule is: $\sigma_p > \sigma_{io} > \sigma_{so} > \sigma_{eo} > \sigma_c$. Although the optical method has the highest sensitivity, it is less applicable because the impeller inlet cannot be visualized on most industrial occasions. The method based on liquid-borne noise is more sensitive than that of solid-borne vibration and airborne noise. This is because the acoustic signal generated by the migration or collapse of bubbles will be received by the hydrophone at the beginning of cavitation. And, due to small amount of bubbles at the inception cavitation, the induced vibration signal acted on the structure will not be received by the vibration acceleration sensor. Moreover, the magnitude

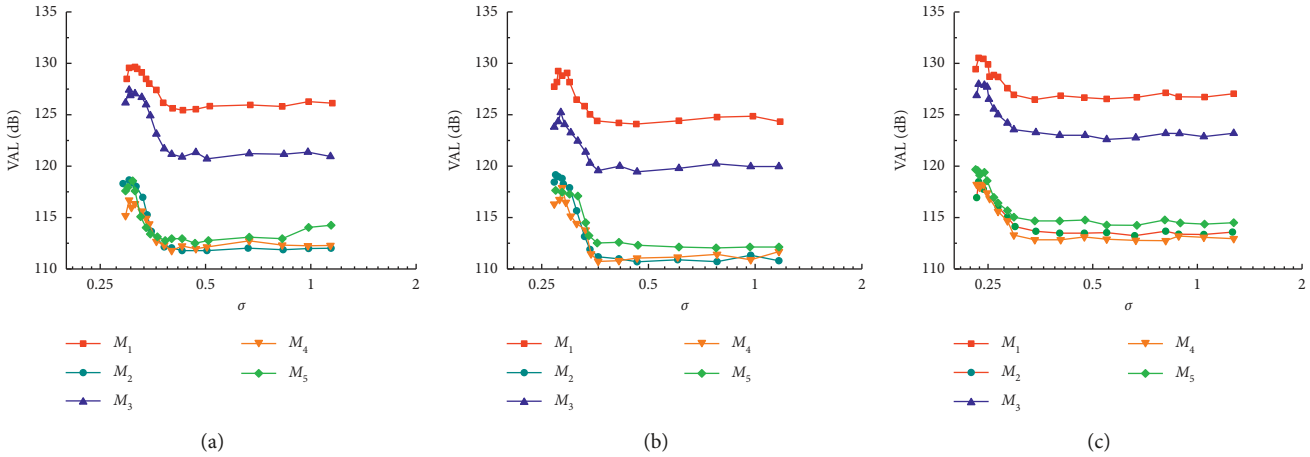

Figure 10: VAL curve of solid-borne vibration for three flow coefficients. (a) $\varphi = 0.098$; (b) $\varphi = 0.065$; (c) $\varphi = 0.032$.

Table 5: Incipient cavitation coefficient based on liquid-borne noise, airborne noise, and solid-borne vibration.

Flow coefficient φ	0.032	0.065	0.098
Incipient cavitation coefficient based on liquid-borne noise σ_{io}	0.282	0.318	0.357
Incipient cavitation coefficient based on airborne noise σ_{eo}	0.275	0.310	0.350
Incipient cavitation coefficient based on solid-borne vibration σ_{so1} at M_1	0.276	0.310	0.341
Incipient cavitation coefficient based on solid-borne vibration σ_{so2} at M_2	0.281	0.311	0.339
Incipient cavitation coefficient based on solid-borne vibration σ_{so3} at M_3	0.280	0.312	0.348
Incipient cavitation coefficient based on solid-borne vibration σ_{so4} at M_4	0.282	0.311	0.339
Incipient cavitation coefficient based on solid-borne vibration σ_{so5} at M_5	0.282	0.312	0.345

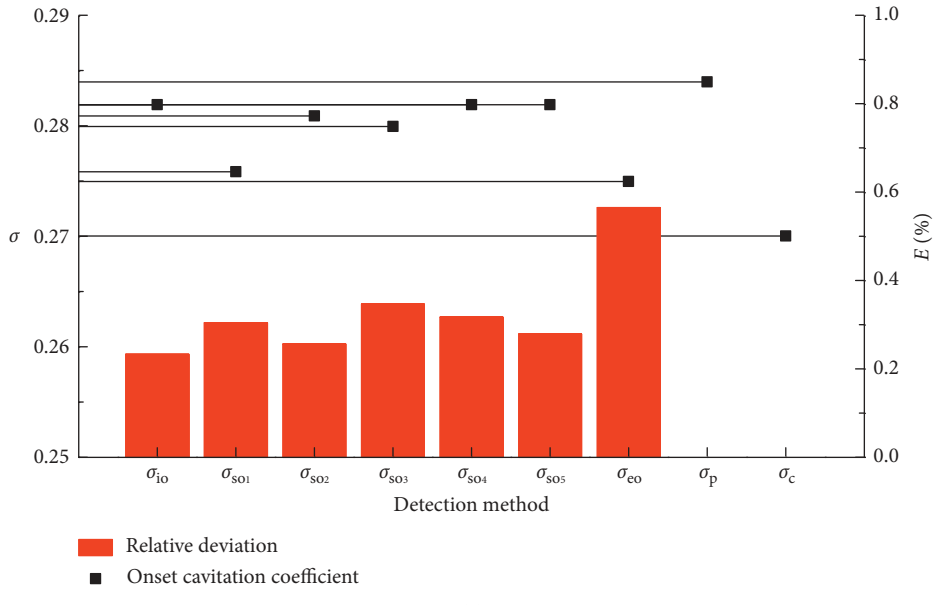

(a)

Figure 11: Continued.

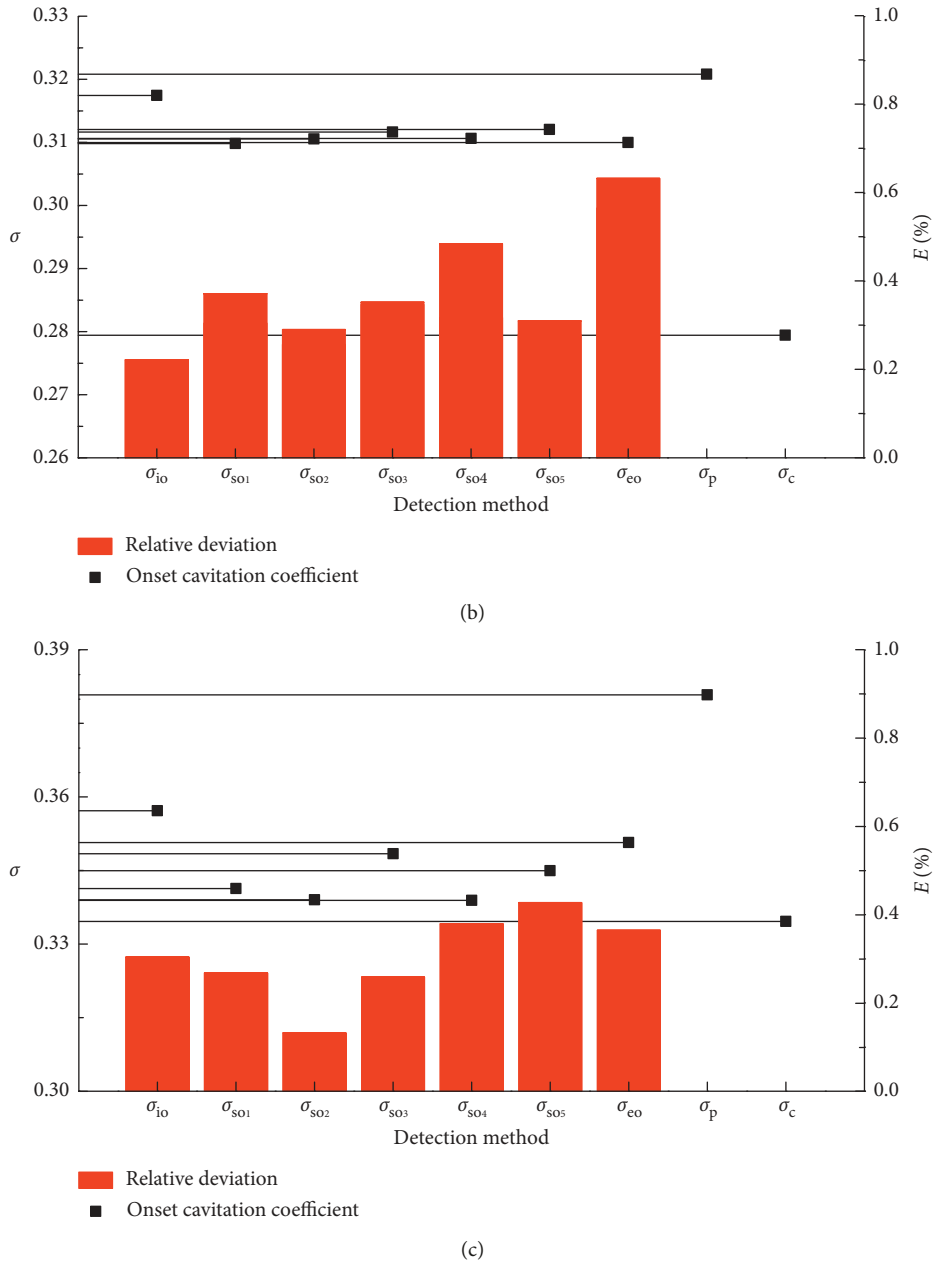

Figure 11: Sensitivity and reliability comparison of different cavitation detection methods. (a) $\varphi = 0.032$; (b) $\varphi = 0.064$; (c) $\varphi = 0.098$.

of air acoustic energy can be ignored compared with that of environmental noise. So, the sound pressure transducer receives a weak cavitation signal.

As for the relative deviation, it is different for various measuring parameters under noncavitation stage. Among them, the maximum relative deviation for liquid-borne noise, solid-borne vibration, and airborne noise is found to be 0.31%, 0.48%, and 0.63%. This suggests the liquid-borne noise signal is best to resist environmental interference. In the process of signal acquisition, the installation type and location of hydrophone can ensure good reception of cavitation acoustic signal and lower the effects from pressure pulsation and pseudo acoustic. On the other hand, due to high impedance produced between different media, the liquid-borne noise is less affected by the background. The vibration coming from the motor or bearing makes the relative deviation of solid-borne vibration of pump larger. And for airborne noise, almost all the environmental factors would cause changes. Therefore, the reliability of airborne noise is lowest for cavitation detection.

In summary, the liquid-borne noise has high anti-interference performance and sensitivity to cavitation signals. Therefore, the incipient cavitation point obtained by liquid-borne noise is used for cavitation stage division.

4. Proposals of New Cavitation Detection Method

The variation of flow rate or decrease of cavitation coefficient would cause a formation of cavitation in the pump, resulting

in a change in the measured magnitude. Although the sensitivity is improved compared with conventional methods, the detection method only relying on the OSPL of liquid-borne noise still has certain limitation. The influence of cavitation on frequency band may be diverse. So, the frequency band, which is high sensitive to cavitation but low to flow rate, is sought. With a certain threshold value, the cavitation stage is determined by the spectrum method.

4.1. Cavitation-Sensitive Frequency Band at Rated Rotating Speed. At the rated rotating speed of 1450 r/min, the 1/3 octave spectrum of liquid-borne noise under different cavitation coefficients and flow coefficients is analyzed in Figure 12, where the centre frequency of 1/3 octave band is plotted on horizontal axis and the OSPL of each 1/3 octave band is calculated. In Figure 12(a), the 1/3 octave spectrum under cavitation coefficient $\sigma = 1.253$ is selected as the standard, and the absolute values of OSPL variation on each frequency band relative to the standard spectrum are normalized for other cavitation coefficients. In Figure 12(b), the spectrum under flow coefficient $\varphi = 0.065$ is selected as the standard, and the absolute values of OSPL variation on each frequency band relative to the standard spectrum are normalized for other flow coefficients. The color denotes the normalized variation, where 0 means no change relative to the standard and 1 means the largest change.

It is obvious the OSPL of liquid-borne noise changes under various cavitation and flow coefficients. However, comparing Figure 12(a) with Figure 12(b), we find the frequency bands affected are diverse. In Figure 12(a), at the initial stage of reducing cavitation coefficient, the change rate relative to the standard value seems to be minor. When the cavitation coefficient drops to 0.38, the change rate increases sharply for high-frequency band between 2000 and 3000 Hz and low-frequency band below 100 Hz but varies little in the medium-frequency band of 100–1000 Hz. In Figure 12(b), the influence of flow on the spectrum is mainly concentrated in the middle and low frequency below 1000 Hz. When the flow changes from rated to off-rated conditions, the OSPL changes significantly below 60 Hz and 100–300 Hz. And with increasing flow coefficient, the change rate gradually increases. At these frequency bands, the axial frequency, blade passing frequency, and their harmonics have nonnegligible impact, which indicates the flow mainly affects discrete eigenvalues in low-frequency band. However, the generation of cavitation not only has a certain influence on discrete eigenvalues in low-frequency band but also has a greater impact on broadband components in high frequency. Moreover, comparing Figure 12(a) with Figure 8, it is seen that at the cavitation coefficient of 0.38, the OSPL of liquid-borne noise remains unchanged, but the OSPLs of the frequency band between 2000 and 3000 Hz have changed significantly. Therefore, the spectral analysis method for cavitation detection is more accurate. And the frequency band of 2000–3000 Hz, which is sensitive to cavitation but not to flow, is selected for further research.

4.2. Cavitation Determination Based on Frequency Quantization. Usually, the rotating speed influences the discrete eigenvalues in the frequency spectrum. To reduce the effect of discrete eigenvalues on sound pressure level of broadband components, the spectrum signal of liquid-borne noise is filtered with a bandwidth of 1 Hz. The SPL of broadband components is obtained as follows:

$$L_{\mathrm{pa}} = 10\lg\left(\sum_{i=1}^{\mathrm{n}} 10^{0.1L_{\mathrm{p}}(f_i)}\right), \tag{4}$$

where f_i is the filter function, by which the original spectrum is filtered to a broadband spectrum with a bandwidth of 1 Hz.

The spectrum of liquid-borne noise under various rotating speeds is processed at the same flow coefficient of 0.065. For quantitative analysis, the band-pass filtering was applied on the frequency bands of 0–100 Hz and 2000–3000 Hz respectively. The broadband SPLs of liquid-borne noise for these frequency bands are shown in Figure 13.

With increasing rotating speed, the broadband SPL shows an increasing trend for the frequency band of 0–100 Hz or 2000–3000 Hz. As the cavitation coefficient decreases, the SPL for the frequency band of 0–100 Hz rises slightly with an obvious fluctuation. This is because the sidelobe frequency existing between discrete eigenvalue in the low-frequency filtering process plays an uncertain role in the broadband SPL. And because the energy of background noise is higher, the cavitation energy is relatively lower in the stages of noncavitation and initial cavitation. When logarithmic processing is carried out with dB as the dimensionless basis, the cavitation noise has less effect than background noise; thus, the broadband SPL does not change significantly in the spectrum. However, for the frequency band of 2000–3000 Hz, since the discrete eigenvalue energy has been attenuated and submerged in the broadband frequency and the background noise level of the frequency band is low in the noncavitation stage, the effect of cavitation is prominent. Moreover, due to wider frequency band and large number of samples after filtering, the broadband SPL fluctuates less when it is not under cavitation.

Based on the average value of SPL at noncavitation stage, the maximum of broadband SPL in the frequency band of 0–100 Hz is only about 0.4% higher than the benchmark, while the maximum in the frequency band of 2000–3000 Hz is about 3.9% higher. Therefore, it is more appropriate to use the 2000–3000 Hz band as the reference band for cavitation determination.

In order to figure out the threshold value for cavitation detection based on the spectrum of liquid-borne noise, the principle of 3σ is introduced, also known as the Pauta principle. Assuming that a certain set of data contains only random error, after calculating the standard deviation, an interval shall be determined according to a certain probability, and the data outside the interval shall be eliminated. In the normal distribution, σ is the standard deviation, μ is the mean value, and $x = \mu$ is the symmetric axis. The 3σ principle means the probability that the value is distributed at $(\mu - 3\sigma, \mu + 3\sigma)$ is 0.9974.

The average value of broadband SPL in the frequency band of 2000–3000 Hz is taken as reference for the cavitation

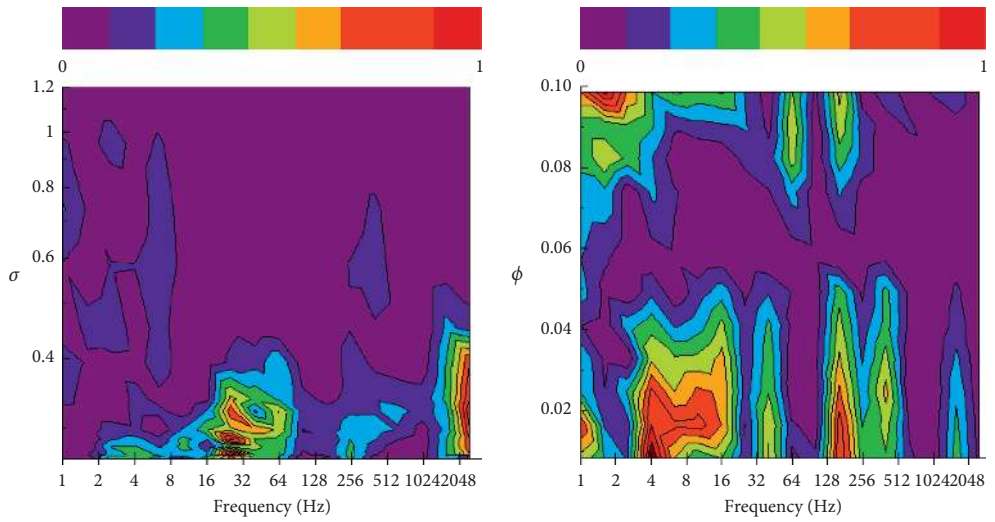

Figure 12: Normalized 1/3 octave spectrum of liquid-borne noise: (a) Under various cavitation coefficients. (b) Under various flow coefficients.

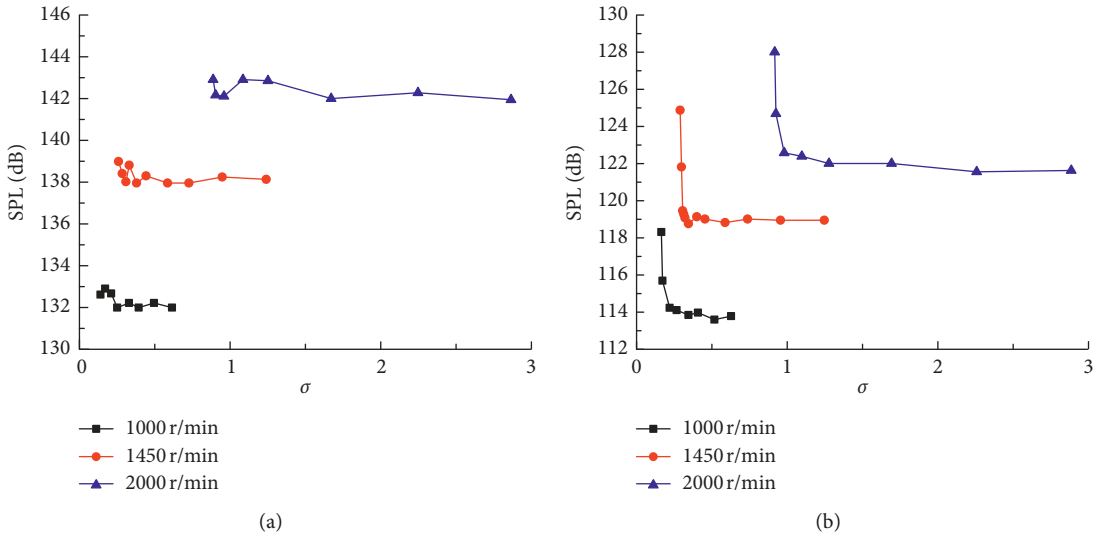

Figure 13: Variation of broadband SPL of liquid-borne noise. (a) 0–100 Hz. (b) 200–3000 Hz.

coefficient larger than σ_p, and the percentage of the change relative to the reference value is used as the threshold. The statistic results are shown in Table 6. To avoid the effect of noise fluctuation on the accuracy of cavitation determination at the stage of noncavitation, the threshold value for 2000–3000 Hz is determined as 1%. In other words, the cavitation is considered to occur when the average SPL at the frequency band is 1% higher than that of noncavitation stage.

5. Verification of Cavitation Detection Method

For verifying the proposed detection method for incipient cavitation, an ultra-low-specific speed volute-type centrifugal pump was studied. Its main design parameters are

Table 6: Threshold value of broadband SPL at different rotating speeds.

Rotating speed ($r \cdot min^{-1}$)	Average $\overline{X}_a$ (%)	Mean square error S_a (%)	Threshold value (%)
1000	1.78	0.30	0.88
1450	1.59	0.21	0.96
2000	2.19	0.41	0.96

$Q_d = 12.5\ m^3/h$, $H_d = 74$ m, $n = 2950$ r/min, and $n_s = 25$. The geometry parameters are shown in Table 7.

5.1. Energy Performance. The cavitation performance curves for various flow coefficients are demonstrated in Figure 14.

Table 7: Main geometry parameters of the pump.

Item	Parameter	Value
Impeller	Inlet diameter, D_1 (mm)	68
	Outlet diameter, D_2 (mm)	228
	Number of blades, z	6
	Wrap angle, θ (°)	145
	Outlet width, b_2 (mm)	7
Volute	Basic diameter, D_3 (mm)	245
	Inlet width, b_3 (mm)	18
	Discharge diameter, D_4 (mm)	32

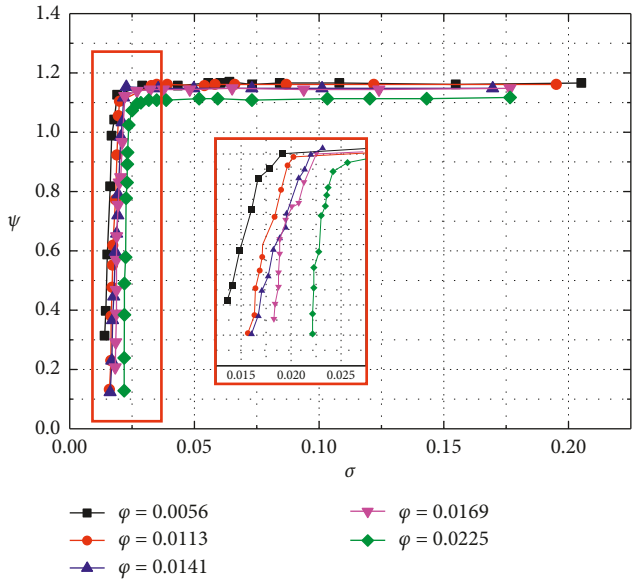

Figure 14: Cavitation performance curves at various flow coefficients.

The critical cavitation coefficients corresponding to 3% drop of head at different flow rates are shown in Table 8.

As can be seen, the slope of cavitation performance curve remains constant at larger cavitation coefficient, indicating the hydraulic performance of the pump is not affected. With the decrease of cavitation coefficient, the cavitation gradually appears in the pump, which leads to the drop of head. At the initial cavitation stage, the change rate is relatively small. While, when it develops to certain extent, the head begins to fall sharply. The drop point of head is different at different flow coefficients, and the head drops earlier at higher flow coefficients than lower conditions, illustrating the cavitation is easy to occur at high flow condition too.

5.2. Cavitation Detection Method Based on Liquid-Borne Noise. The OSPL of liquid-borne noise with decreasing cavitation coefficient at various flow coefficients is demonstrated in Figure 15(a). Correspondingly, the normalized 1/3 octave spectrum at rated flow condition is illustrated in Figure 15(b) for various cavitation coefficients. The 1/3 octave spectrum at $\sigma = 1.253$ is used for standard, and the absolute values of OSPL variation on each frequency band

Table 8: Critical cavitation coefficients based on the energy detection method.

Flow coefficient φ	0.0056	0.0113	0.0141	0.0169	0.0225
Critical cavitation coefficient σ_c	0.017	0.018	0.020	0.021	0.026

relative to the standard spectrum are normalized. The color denotes the normalized variation, where 0 means no change relative to the standard and 1 means the largest change.

The enlarged flow design method is employed to design the ultralow-specific centrifugal pump. The design process of this method can be found in the literature [25]. So, the pump efficiency does not reach maximum under the rated condition. With the flow coefficient increasing from 0.0056 to 0.0225, the efficiency of pump increases gradually. The increase in efficiency means that more energy is converted to the kinetic energy of fluid, while other forms of energy are reduced. As can be seen from Figure 15(a), when the cavitation coefficient is greater than the incipient cavitation coefficient based on liquid-borne noise, the OSPL decreases gradually with increasing flow coefficient. While when it is less than the incipient cavitation coefficient, the OSPL firstly increases to a certain degree at the critical cavitation coefficient and then begins to decline. From Figure 15(b), when the cavitation coefficient equals to 0.029, the liquid-borne noise basically exhibits a high sensitivity to cavitation in the whole frequency band. Especially in the frequency band between 2000 Hz and 3000 Hz, the change gradient of OSPL is largest. However, in most frequency bands below 2000 Hz, when the cavitation coefficient declines to a certain value, the variation law of OSPL is not consistent and monotonous. Therefore, it is verified that for the liquid-borne noise, the frequency band of 2000–3000 Hz has the highest sensitivity to cavitation and is suitable for the cavitation determination.

The frequency band of 2000–3000 Hz is used for cavitation determination. And the change rate of 1% for broadband SPL is seen as the threshold. To verify the accuracy of the threshold value, the frequency band between 2000 and 3000 Hz at the rated condition was filtered with a bandwidth of 1 Hz, and the broadband SPL was calculated, as shown in Figure 16. As can be seen, firstly, the broadband SPL increases at the flow coefficient of 0.0225, while finally it increases for $\varphi = 0.0056$. And the broadband SPL under larger flow is smaller than that under smaller flow, indicating the flow has certain influence on the broadband SPL.

With the OSPL increased by 0.5% compared with the reference as the incipient cavitation, the incipient cavitation coefficients σ_{io} are found. Moreover, with 1% of change rate of broadband SPL as the threshold, the incipient cavitation coefficients are shown in Table 9. Comparing Tables 8 and 9, the incipient cavitation coefficient based on the threshold is advanced than other methods.

6. Conclusions

Based on the experiments on a visual closed test rig, the cavitation incipient point was defined by different methods.

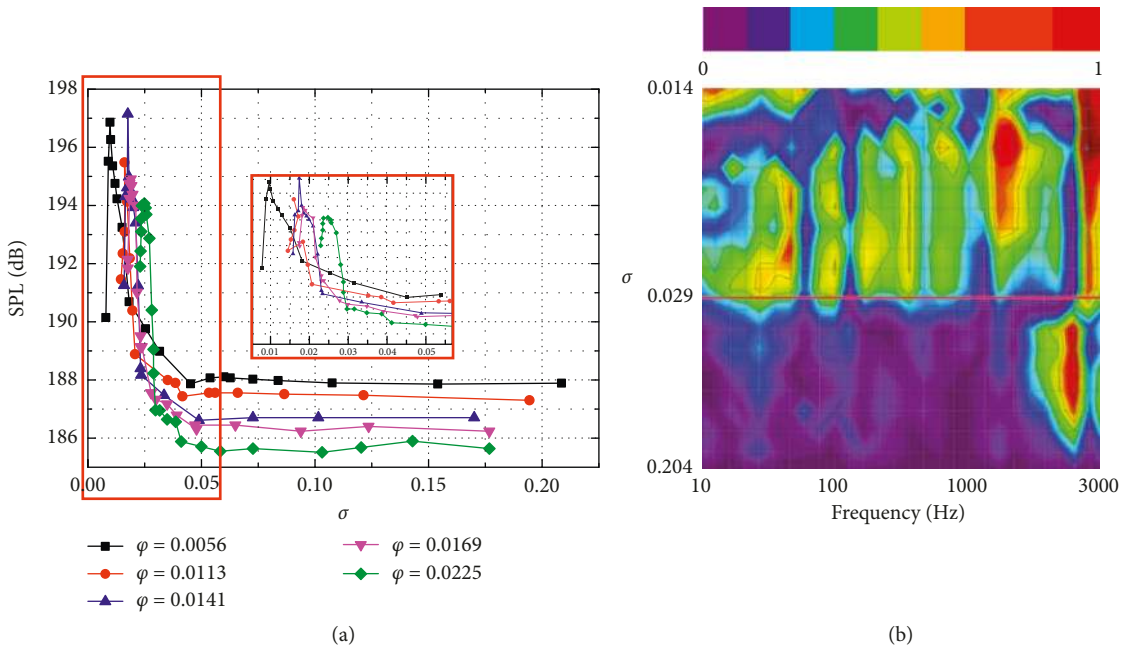

Figure 15: OSPL curve and normalized 1/3 octave spectrum of liquid-borne noise. (a) OSPL curve under different flow coefficients. (b) Normalized 1/3 octave spectrum at rated flow coefficient.

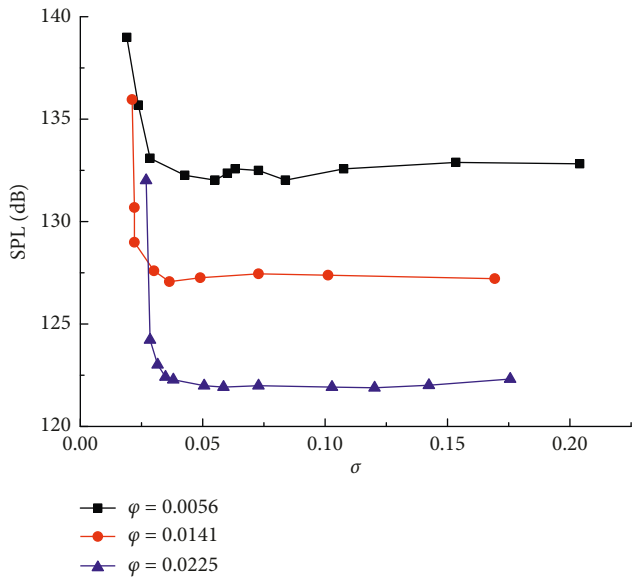

Figure 16: Broadband SPL of liquid-borne noise at 2000–3000 Hz.

Table 9: Incipient cavitation coefficients based on flow-borne noise at different flow coefficients.

Flow coefficient φ	0.0056	0.0113	0.0141	0.0169	0.0225
Incipient cavitation coefficient based on OSPL σ_{io}	0.022	0.025	0.028	0.031	0.033
Incipient cavitation coefficient based on breadboard SPL σ_{iob}	0.022	—	0.029	—	0.033

A more accurate inception cavitation method based on flow-borne noise was determined compared to other cavitation determination methods. Then, through processing and analysis of noise spectrum, the frequency band with high sensitivity to cavitation was found, and the cavitation threshold of broadband frequency was quantified. Based on this, the cavitation determination based on the broadband SPL of liquid-borne noise is proposed.

(1) When a small amount of bubbles is observed through high-speed photography, the pump head remains unchanged just like noncavitation condition. With decreasing cavitation coefficient, the total levels of liquid-borne noise, airborne noise, and solid-borne vibration firstly increase and then decrease. The incipient cavitation coefficients obtained by different detection methods are different, and the rule is: $\sigma_p > \sigma_{io} > \sigma_{so} > \sigma_{eo} > \sigma_c$. Although the optical method has the highest sensitivity, it is less applicable because the impeller inlet cannot be visualized on most industrial occasions. The method based on liquid-borne noise is more sensitive and reliable than that of solid-borne vibration and airborne noise, although less appropriate for small pumps in comparison with the airborne SPL.

(2) The spectra of flow-borne noise influenced by cavitation are mainly concentrated in the frequency band of 2000–3000 Hz and below 100 Hz. While for flow, it is concentrated in the middle and low frequency below 1000 Hz. At the cavitation coefficient of 0.38, the OSPL of liquid-borne noise remains unchanged, but the OSPLs of the frequency band between 2000 and 3000 Hz have changed significantly. And due to more vital cavitation effect compared with 0–100 Hz, the frequency band of 2000–3000 Hz, which is sensitive to cavitation but not to flow, is determined for inception cavitation detection. Introducing into the principle of 3σ, the threshold value for 2000–3000 Hz based on the spectrum of liquid-borne noise is determined as 1%.

(3) The frequency band of 2000–3000 Hz and the change rate of 1% for broadband SPL were further verified on an ultra-low-specific speed pump ($n_s = 25$). The incipient cavitation coefficient based on the threshold is advanced than other methods; especially, its sensitivity has been greatly improved.

Data Availability

The experimental data used to support the findings of this study were supplied by the research group of Jiangsu University under license, so we still cannot put them into the system, and the requests for access to these data should be made to the corresponding author.

Conflicts of Interest

The authors declare that there are no conflicts of interest regarding the publication of this paper.

Acknowledgments

This work was supported by the National Natural Science Foundation of China (nos. 51879122, 51509111, and 51779106), China Postdoctoral Science Foundation (2017M611721), Association Innovation Fund of Production, Learning, and Research (BY2016072-01), Zhenjiang Key Research and Development Plan (GY2017001 and GY2018025), Open Research Subject of Key Laboratory of Fluid and Power Machinery, Ministry of Education, Xihua University (szjj2015-017, szjj2017-094, and szjj2016-068), Sichuan Provincial Key Lab of Process Equipment and Control (GK201614 and GK201816), Advanced Talent Foundation of Jiangsu University (15JDG052), and a project funded by the Priority Academic Program Development of Jiangsu Higher Education Institutions (PAPD) and Jiangsu Top Six Talent Summit Project (GDZB-017).

References

[1] B. Qing, B. Yu, W. Lan et al., "Measurement of cavitation noise in centrifugal pump," *Journal of Drainage and Irrigation Machinery Engineering*, vol. 34, no. 3, pp. 198–203, 2016.

[2] Y. Wang, Y. Zhao, L. Dong et al., "Cavitation characteristics of ultra-low specific speed centrifugal pump based on fluid-acoustic coupling method," *Transaction of the Chinese Society for Agricultural Machinery*, vol. 48, no. 12, pp. 114–123, 2017.

[3] L. Dong, Y. Zhao, and D. Cui, "Research on cavitation acoustic characteristics of centrifugal pump based on fluid-acoustic field coupling method," *Advances in Mechanical Engineering*, vol. 10, no. 5, article 1687814018773665, 2018.

[4] M. Savar, H. Kozmar, and I. Sutlovic, "Improving centrifugal pump efficiency by impeller trimming," *Desalination*, vol. 249, no. 2, pp. 654–659, 2009.

[5] Y. Su, Y. Wang, X. Duan et al., "Cacitation experimental research on centrifugal pump," *Transaction of the Chinese Society for Agricultural Machinery*, vol. 41, no. 3, pp. 77–80, 2010.

[6] X. Guo, L. Zhu, Z. Zhu, B. Cui, and Y. Li, "Numerical and experimental investigations on the cavitation characteristics of a high-speed centrifugal pump with a splitter-blade inducer," *Journal of Mechanical Science and Technology*, vol. 29, no. 1, pp. 259–267, 2015.

[7] N. Qiu, *Experimental Research on Cavitation Erosion of Impeller Materials*, Zhejiang Univercity, Hangzhou, China, 2016.

[8] X. Li, B. Yu, Y. Ji, J. Lu, and S. Yuan, "Statistical characteristics of suction pressure signals for a centrifugal pump under cavitating conditions," *Journal of Thermal Science*, vol. 26, no. 1, pp. 47–53, 2017.

[9] L. Alfayez, D. Mba, and G. Dyson, "The application of acoustic emission for detecting incipient cavitation and the best efficiency point of a 60 kW centrifugal pump: case study," *NDT & E International*, vol. 38, no. 5, pp. 354–358, 2005.

[10] T. Alhashan, "Monitoring of bubble formation during the boiling process using acoustic emission signals," *International Journal of Engineering Research & General Science*, vol. 2, no. 4, pp. 66–72, 2016.

[11] A. Kotb and A. M. Abdulaziz, "Cavitation detection in variable speed pump by analyzing the acoustic and vibration spectrums," *Engineering*, vol. 07, no. 10, pp. 706–716, 2015.

[12] X. Duan, Y. Wang, and Y. Su, "Vibration analysis applied cavitation monitoring of a centrifugal pump," *Journal of Vibration and Shock*, vol. 30, no. 4, pp. 161–165, 2011.

[13] B. Bajic and A. Keller, "Spectrum normalization method in vibro-acoustical diagnostic measurements of hydroturbine cavitation," *Journal of Fluids Engineering*, vol. 118, no. 4, pp. 756–761, 1996.

[14] B. Bajic, "Methods for vibro-acoustic diagnostics of turbine cavitation," *Journal of Hydraulic Research*, vol. 41, no. 1, pp. 87–96, 2003.

[15] J. Friedrich, "Diagnosis of cavitation in centrifugal pumps," *Sulzer Technical Review*, vol. 74, pp. 29–35, 1992.
[16] M. Čdina, "Detection of cavitation phenomenon in a centrifugal pump using audible sound," *Mechanical Systems & Signal Processing*, vol. 17, no. 6, pp. 1335–1347, 2003.
[17] M. Čudina and J. Prezelj, "Detection of cavitation in situ operation of kinetic pumps: effect of cavitation on the characteristic discrete frequency component," *Applied Acoustics*, vol. 70, no. 9, pp. 1175–1182, 2009.
[18] T. Rus, M. Dular, B. Sirok, M. Hocevar, and I. Kern, "An investigation of the relationship between acoustic emission, vibration, noise and cavitation structures on a Kaplan turbine," *Journal of Fluids Engineering*, vol. 129, no. 9, pp. 1112–1122, 2007.
[19] X. Escaler, E. Egusquiza, M. Farhat, F. Avellan, and M. Coussirat, "Detection of cavitation in hydraulic turbines," *Mechanical Systems and Signal Processing*, vol. 20, no. 4, pp. 983–1007, 2006.
[20] X. Duan, Y. Wang, and Y. Su, "Features combined classification of cavitation in waterjet pumps," *Journal of Shanghai Jiaotong University*, vol. 45, no. 9, pp. 1322–1326, 2011.
[21] Y. Su, Y. Wang, and X. Duan, "Research on the cavitation identification experimentation of marine waterjet," *Journal of Shanghai Jiaotong University*, vol. 46, no. 3, pp. 404–409, 2012.
[22] Z. Pu, W. Zhang, K. Shi et al., "Turbine cavitation testing based on wavelet singularity detection," *Journal of Vibration and Shock*, vol. 24, no. 5, pp. 74–76, 2005.
[23] H. Shi, Z. Li, and Y. Liu, "Investigation on cavitation characteristics in hydraulic turbines based on frequency bandwidth analysis of wavelet packet," *Large Electric Machine and Hydraulic Turbine*, no. 1, pp. 43–48, 2009.
[24] F. Tao, K. Liu, X. Li et al., "Development of the experimental system for measuring the hydrodynamic noise in centrifugal pump," *Fluid Machinery*, vol. 33, no. 4, pp. 27–30, 2005.
[25] Y. Y. Ni, S. Yuan, and J. Yuan, "Research on enlarged flow design for low specific-speed centrifugal pump," *China Rural Water and Hydropower*, no. 8, pp. 126–129, 2007.